Supplementary Information

High-performance liquid chromatography mass spectrometry of gold and alloy clusters protected by hydrophilic thiolates

Yoshiki Niihori,[a] Daisuke Shima,[a] Kana Yoshida,[a] Kota Hamada,[a] Lakshmi V. Nair,[a] Sakiat Hossain,[b] Wataru Kurashige[a] and Yuichi Negishi*[a,b]

[a]Department of Applied Chemistry, Faculty of Science, Tokyo University of Science, 1−3 Kagurazaka, Shinjuku−ku, Tokyo 162−8601, Japan.
[b]Photocatalysis International Research Center, Tokyo University of Science, 2641 Yamazaki, Noda, Chiba 278–8510, Japan.
Corresponding Author E-mail: negishi@rs.kagu.tus.ac.jp; Tel: +81–3–5228–9145; Fax: +81–3–5261–4631

1. Additional Tables

Table S1. Number of Au Atoms and Ligands, Charge States, and Estimated Number of Valence Electrons for $Au_n(SG)_m$ Clusters Observed in LC/MS Experiments.

Number of Au atoms [a]	Number of ligands [a]	Charge states [a]	Number of valence electrons [b]	Intensity [c]
10	10	0	- [d]	strong
10	11	-1	- [d]	weak
11	11	0	- [d]	strong
11	12	-1	- [d]	weak
12	12	0	- [d]	strong
12	13	-1	- [d]	weak
13	13	0	- [d]	weak
13	14	-1	- [d]	weak
15	13	0	2	strong
16	14	0	2	middle
16	15	-1	2	weak
17	14	-1	4	weak
18	14	0	4	strong
18	15	-1	4	middle
19	15	0	4	middle
19	16	-1	4	weak
20	16	0	4	middle
20	17	-1	4	weak
21	16	-1	6	weak
21	17	0	4	weak
22	16	0	6	weak
22	17	-1	6	middle
23	17	0	6	strong
24	18	0	6	middle
25	18	-1	8	strong
25	20	-1	6	weak
26	19	-1	8	weak
27	19	0	8	weak
27	20	-1	8	weak
29	20	-1	10	strong
30	21	-1	10	middle

31	22	-1	10	middle
32	22	0	10	middle
32	23	-1	10	middle
33	22	-1	12	strong
33	23	0	10	middle
34	23	-1	12	strong
34	24	0	10	weak
34	25	-1	10	weak
35	22	-1	14	weak
35	24	-1	12	middle
36	23	-1	14	weak
36	24	0	12	weak
36	25	-1	12	weak
37	24	-1	14	strong
37	25	0	12	weak
38	24	0	14	strong
38	25	-1	14	middle
39	24	-1	16	strong
39	25	-[e]	-[e]	weak
39	26	-[e]	-[e]	weak
40	25	-[e]	-[e]	weak
40	26	-[e]	-[e]	weak
40	27	-[e]	-[e]	weak
41	26	-[e]	-[e]	strong
42	26	-[e]	-[e]	weak
42	27	-[e]	-[e]	middle
43	26	-[e]	-[e]	weak
43	27	-[e]	-[e]	weak
44	27	-[e]	-[e]	middle
44	28	-[e]	-[e]	weak
45	27	-[e]	-[e]	weak
45	28	-[e]	-[e]	weak
46	28	-[e]	-[e]	strong
46	29	-[e]	-[e]	middle
47	28	-[e]	-[e]	middle
47	29	-[e]	-[e]	weak
48	29	-[e]	-[e]	middle
49	29	-[e]	-[e]	weak
49	30	-[e]	-[e]	weak
50	30	-[e]	-[e]	weak
51	30	-[e]	-[e]	weak
52	31	-[e]	-[e]	weak
54	31	-[e]	-[e]	weak

[a]These values were estimated by the analyses of ESI mass spectra (Figure 1 and S11–S13). [b]These values were estimated using the equation described in literature[1] on the basis of the number of Au atoms and ligands and the charge states. [c]Ion intensities in mass spectra. [d]These species are considered to be metal–thiolate complex without metal core. [e]For these clusters, it is difficult to estimate the charge state and thereby the number of valence electrons with confidence because of quite a low ion intensity in the mass spectra.

Table S2. Number of Metal Atoms and Ligands, Charge States, and Estimated Number of Valence Electrons for $Au_{n-x}Ag_x(SG)_m$ Clusters Observed in LC/MS Experiments.

Number of				Charge states [a]	Number of valence electrons [b]	Experimental condition [c]	Intensity [d]
Metal	Au	Ag	Ligands				
10	9	1	10	0	- [e]	I, II, III	strong
10	8	2	10	0	- [e]	I, II, III	strong
10	7	3	10	0	- [e]	III	strong
10	6	4	10	0	- [e]	III	strong
11	10	1	11	0	- [e]	I, II, III	strong
11	9	2	11	0	- [e]	I, II, III	strong
11	8	3	11	0	- [e]	III	strong
11	7	4	11	0	- [e]	III	strong
11	6	5	11	0	- [e]	III	strong
12	11	1	12	0	- [e]	I, II, III	strong
12	10	2	12	0	- [e]	I, II, III	strong
12	9	3	12	0	- [e]	III	strong
15	14	1	13	0	2	I, II, III	strong
15	13	2	13	0	2	I, II, III	strong
15	12	3	13	0	2	I, II, III	strong
15	11	4	13	0	2	III	strong
16	15	1	14	0	2	I, II	weak
16	14	2	14	0	2	I	weak
18	17	1	14	0	4	I, II	strong
18	16	2	14	0	4	I, II, III	strong
18	15	3	14	0	4	II, III	strong
18	14	4	14	0	4	II, III	strong
18	13	5	14	0	4	III	strong
18	12	6	14	0	4	III	strong
18	16	2	15	-1	4	II, III	middle
18	15	3	15	-1	4	II, III	middle
18	14	4	15	-1	4	III	middle
18	13	5	15	-1	4	III	middle
19	18	1	15	0	4	I, II	weak
19	17	2	15	0	4	I, II	weak
19	16	3	15	0	4	II	weak
19	15	4	16	-1	4	III	weak
19	14	5	16	-1	4	III	weak
19	13	6	16	-1	4	III	weak
19	12	7	16	-1	4	III	weak
20	19	1	15	-1	6	I, II	weak
20	19	1	16	0	4	II	weak
21	20	1	16	-1	6	I, II, III	middle
21	19	2	16	-1	6	I, II, III	middle
21	18	3	16	-1	6	I, II, III	middle
21	17	4	16	-1	6	II, III	middle
21	16	5	16	-1	6	III	middle
22	21	1	16	0	6	I, II	weak
22	20	2	16	0	6	I, II	weak
22	21	1	17	-1	6	I	weak
22	20	2	17	-1	6	I	weak
22	19	3	17	-1	6	I	weak
22	18	4	17	-1	6	II, III	weak
22	17	5	17	-1	6	II, III	weak
22	16	6	17	-1	6	II, III	weak
22	15	7	17	-1	6	II, III	weak
23	22	1	17	0	6	I, II	strong
23	21	2	17	0	6	I, II	strong
23	20	3	17	0	6	II, III	strong
23	19	4	17	0	6	II, III	strong
23	18	5	17	0	6	II, III	strong
23	17	6	17	0	6	III	strong
23	17	6	18	-1	6	III	middle

23	16	7	18	-1	6	III	middle
23	15	8	18	-1	6	III	middle
24	23	1	18	0	6	I	weak
24	22	2	18	0	6	I	weak
24	21	3	18	0	6	II	weak
24	20	4	18	0	6	II	weak
24	19	5	18	0	6	II	weak
25	24	1	18	-1	8	I, II	strong
25	23	2	18	-1	8	I, II	strong
25	22	3	18	-1	8	I, II, III	strong
25	21	4	18	-1	8	I, II, III	strong
25	20	5	18	-1	8	II, III	strong
25	19	6	18	-1	8	II, III	strong
25	18	7	18	-1	8	III	strong
25	17	8	18	-1	8	III	strong
26	25	1	18	0	8	I	weak
29	28	1	20	-1	10	I, II	strong
29	27	2	20	-1	10	I, II	strong
29	26	3	20	-1	10	I, II, III	strong
29	25	4	20	-1	10	III	strong
29	24	5	20	-1	10	III	strong
29	23	6	20	-1	10	III	strong
29	22	7	20	-1	10	III	strong
29	21	8	20	-1	10	III	strong
29	20	9	20	-1	10	III	strong

[a]These values were estimated by the analyses of negative-ion ESI mass spectra (Figures S24–S26). [b]These values were estimated using the equation described in literature[1] on the basis of the number of Au atoms and ligands and the charge states. [c]Initial metal ion ratios of $[HAuCl_4]$:$[AgNO_3]$. I–III represents 24.5:0.5, 23:2, and 21:4, respectively. [d]Ion intensities in mass spectra. [e]These species are considered to be metal–thiolate complex without metal core.

Table S3. Number of Metal Atoms and Ligands, Charge States, and Estimated Number of Valence Electrons for $Au_{n-x}Cu_x(SG)_m$ Clusters Observed in LC/MS Experiments.

Number of				Charge states [a]	Number of valence electrons [b]	Experimental condition [c]	Intensity [d]
Metal	Au	Cu	ligands				
9	5	4	10	-1	- [e]	II, III	weak
11	10	1	10	-1	- [e]	III	weak
12	11	1	11	-1	- [e]	II, III	weak
13	11	2	12	-1	- [e]	III	middle
14	13	1	13	-1	- [e]	III	weak
14	12	2	13	-1	- [e]	II, III	weak
15	14	1	13	0	2	I, II, III	strong
15	13	2	13	0	2	III	strong
15	12	3	13	0	2	III	strong
15	14	1	14	-1	- [e]	I, II	weak
15	13	2	14	-1	- [e]	I	weak
17	16	1	14	-1	4	I, II, III	middle
17	15	2	14	-1	4	III	middle
18	17	1	14	0	4	II, III	strong
18	16	2	14	0	4	II, III	strong
18	15	3	14	0	4	III	strong
18	17	1	15	-1	4	I, II, III	middle
20	19	1	13	-1	8	I, II	weak
20	19	1	15	-1	6	II, III	weak
20	18	2	15	-1	6	II, III	weak
21	19	2	15	0	6	III	weak
21	18	3	15	0	6	III	weak
21	17	4	15	0	6	III	weak
21	20	1	16	-1	6	I, II, III	middle
21	19	2	18	-1	4	II, III	middle
22	21	1	16	0	6	I, II, III	weak
22	20	2	16	0	6	II, III	weak
22	21	1	17	-1	6	I, II, III	middle
23	22	1	17	0	6	I, II, III	strong
23	21	2	17	0	6	I, II, III	strong
23	22	1	18	-1	6	I, II, III	middle
23	21	2	18	-1	6	I, II	middle
24	23	1	18	0	6	I	middle
24	22	2	18	0	6	I, II, III	middle
25	24	1	18	-1	8	I, II, III	strong
25	23	2	18	-1	8	I, II, III	strong
25	22	3	18	-1	8	II, III	strong
25	21	4	18	-1	8	II, III	strong
25	20	5	18	-1	8	III	strong
26	22	4	20	0	6	III	weak
26	21	5	20	0	6	III	weak
27	22	5	20	-1	8	III	weak
27	21	6	20	-1	8	III	weak
28	24	4	20	0	8	III	weak
29	28	1	20	-1	10	I, II, III	strong
29	27	2	20	-1	10	III	strong
29	26	3	20	-1	10	III	strong
29	25	4	20	-1	10	III	strong
29	24	5	20	-1	10	III	strong

[a]These values were estimated by the analyses of negative-ion ESI mass spectra (Figures S32 and S33). [b]These values were estimated using the equation described in literature[1] on the basis of the number of Au atoms and ligands and the charge states. [c]Initial metal ion ratios of $[HAuCl_4]$:$[CuCl_2]$. I–III represents 24.5:0.5, 23:2, and 21:4, respectively. [d]Ion intensities in mass spectra. [e]These species are considered to be metal–thiolate complex without metal core.

Table S4. Number of Metal Atoms and Ligands, Charge States, and Estimated Number of Valence Electrons for $Au_{n-x}Pd_x(SG)_m$ Clusters Observed in LC/MS Experiments.

Number of				Charge states [a]	Number of valence electrons [b]	Experimental condition [c]	Intensity [d]
Metal	Au	Pd	Ligands				
6	4	2	8	0	- [e]	II	strong
7	2	5	12	0	- [e]	II	strong
9	8	1	10	0	- [e]	I	middle
9	7	2	10	0	- [e]	I	weak
10	9	1	10	-1	- [e]	I, II	strong
11	10	1	11	-1	- [e]	I, II	strong
12	8	4	14	0	- [e]	II	weak
13	12	1	12	0	- [e]	II	weak
13	10	3	14	0	- [e]	I, II	weak
14	12	2	14	0	- [e]	I, II	weak
14	11	3	14	-1	- [e]	I	weak
15	14	1	13	-2	3	I, II	strong
15	14	1	14	0	- [e]	I, II	middle
16	15	1	15	0	- [e]	II	weak
17	16	1	16	0	- [e]	I	weak
17	15	2	16	-1	- [e]	II	middle
18	17	1	14	-1	4	II	strong
18	16	2	14	-3	5	I, II	strong
18	17	1	16	-1	- [e]	II	weak
18	16	2	17	-1	- [e]	II	middle
19	18	1	15	-1	4	I	weak
19	18	1	16	0	2	I, II	weak
19	17	2	16	-1	2	I	weak
19	18	1	17	-1	2	I, II	weak
20	18	2	17	-1	2	I	weak
20	17	3	18	-1	0	II	weak
21	20	1	17	-1	4	I, II	weak
21	19	2	17	0	2	II	weak
21	19	2	18	-1	2	I, II	weak
23	22	1	17	-1	6	I	weak
23	22	1	18	0	4	I, II	weak
23	20	3	19	-1	2	II	middle
25	24	1	18	-2	8	I, II	strong
25	24	1	19	-1	6	I	middle
25	23	2	20	-1	4	II	middle
26	25	1	20	-1	6	I	middle
29	28	1	20	-1	10	I	strong

[a]These values were estimated by the analyses of negative-ion ESI mass spectra (Figures S39 and S40). [b]These values were estimated using the equation described in literature[1] on the basis of the number of Au atoms and ligands and the charge states. [c]Initial metal ion ratios of $[HAuCl_4]$:$[PdCl_2 \cdot 2NaCl]$. I, II represents 24.5:0.5 and 21:4, respectively. [d]Ion intensities in mass spectra. [e]These species are considered to be metal–thiolate complex without metal core.

2. Additional Schemes

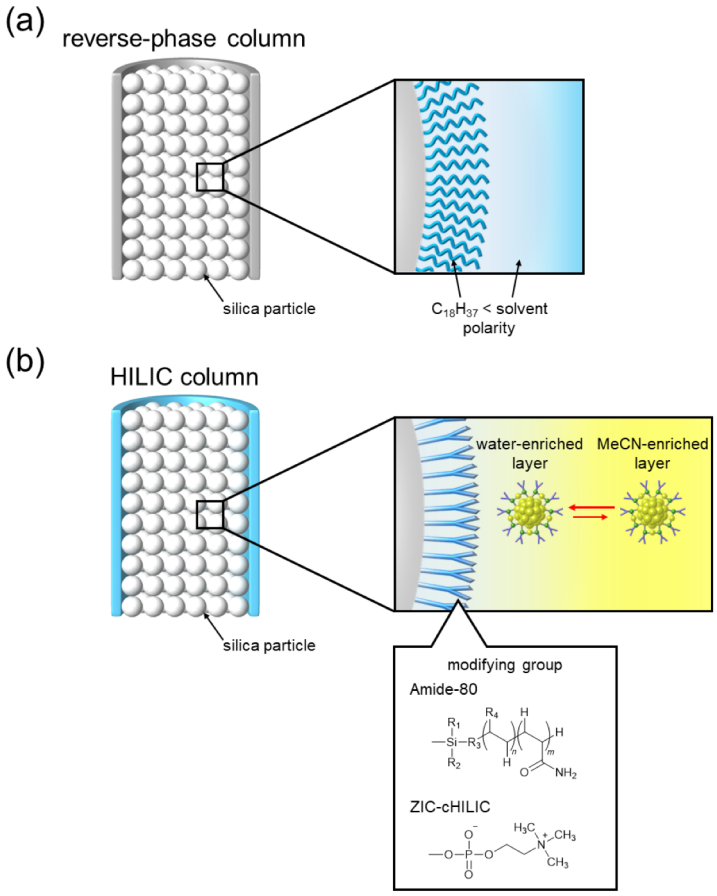

Scheme S1. Comparison of HPLC columns. (a) Reverse-phase column and (b) HILIC column.[2]

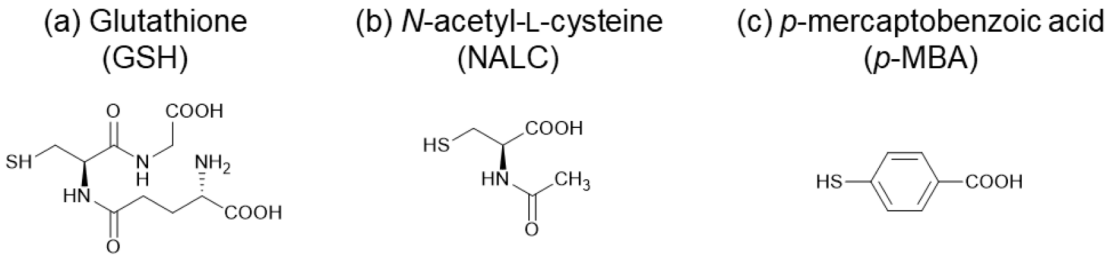

Scheme S2. Structures of thiols used in this work. (a) Glutathione (GSH),[3] (b) *N*-acetyl-L-cysteine (NALC),[4] and (c) *p*-mercaptobenzoic acid (*p*-MBA)[5].

3. Additional Figures

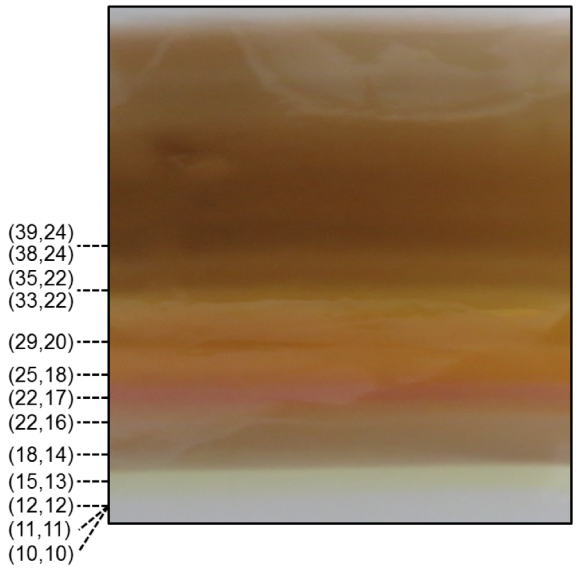

Figure S1. PAGE photograph of as-prepared $Au_n(SG)_m$ clusters used in the experiment depicted in Figure 1 and 2. The tentative assignments of $Au_n(SG)_m$ clusters in the literature[3] are described in the form of (n, m) on the left.

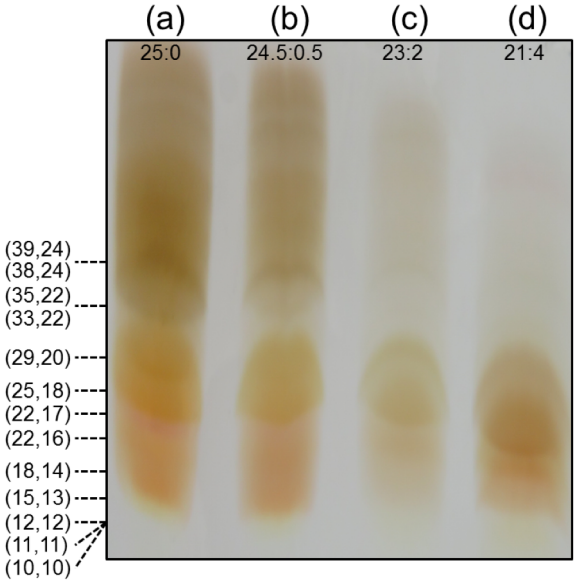

Figure S2. PAGE photograph of as-prepared $Au_{n-x}Ag_x(SG)_m$ clusters used in the experiments illustrated in Figure 5(a) and 6(a); $[HAuCl_4]$:$[AgNO_3]$ = (a) 25:0, (b) 24.5:0.5, (c) 23:2, and (d) 21:4. The tentative assignments of $Au_n(SG)_m$ clusters in the literature[3] are described in the form of (n, m) on the left.

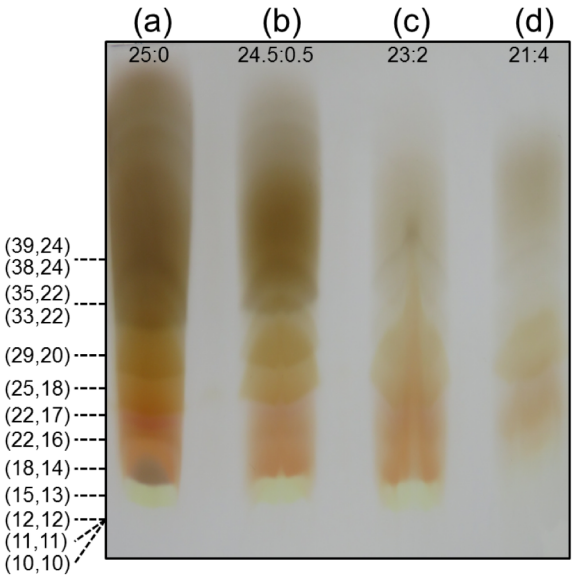

Figure S3. PAGE photograph of as-prepared $Au_{n-x}Cu_x(SG)_m$ clusters used in the experiments shown in Figure 5(b) and 6(b); $[HAuCl_4]$:$[CuCl_2]$ = (a) 25:0, (b) 24.5:0.5, (c) 23:2, and (d) 21:4. The tentative assignments of $Au_n(SG)_m$ clusters in the literature[3] are described in the form of (*n*, *m*) on the left.

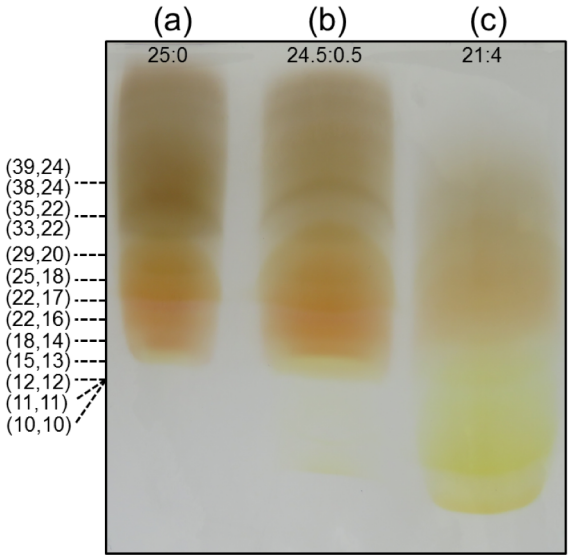

Figure S4. PAGE photograph of as-prepared $Au_{n-x}Pd_x(SG)_m$ clusters used in the experiments depicted in Figure 5(c) and 6(c); $[HAuCl_4]$:$[PdCl_2 \cdot 2NaCl]$ = (a) 25:0, (b) 24.5:0.5, and (c) 21:4. The tentative assignments of $Au_n(SG)_m$ clusters in the literature[3] are described in the form of (*n*, *m*) on the left.

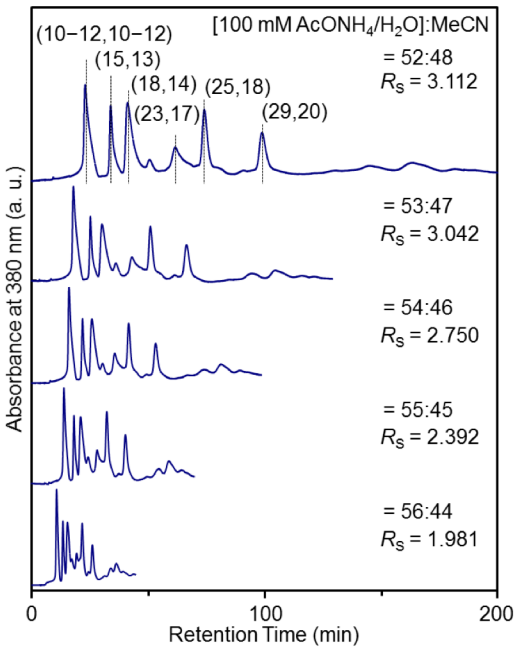

Figure S5. Dependence of the chromatograms of $Au_n(SG)_m$ clusters on the mobile phase in the experiments using an Amide-80 column. R_s indicates the resolution estimated using peaks of $Au_{10–12}(SG)_{10–12}$ and $Au_{15}(SG)_{13}$.[6] In the chromatogram, the peak position of each $Au_n(SG)_m$ cluster is described in the form of (n, m).

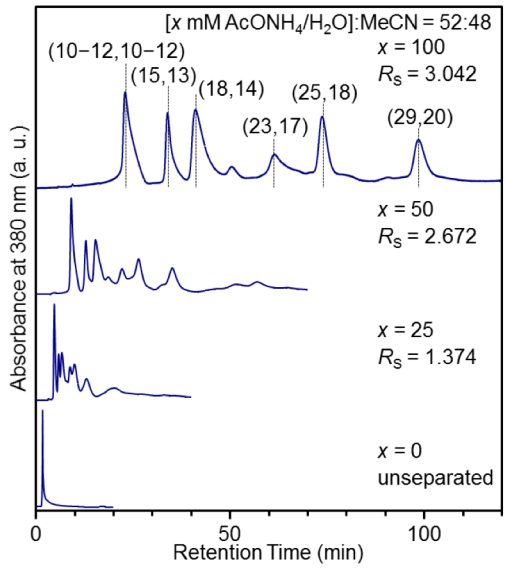

Figure S6. Dependence of the chromatograms of $Au_n(SG)_m$ clusters on the concentration of $AcONH_4$. R_s indicates the resolution estimated using peaks of $Au_{10–12}(SG)_{10–12}$ and $Au_{15}(SG)_{13}$.[6] In the chromatogram, the peak position of each $Au_n(SG)_m$ cluster is described in the form of (n, m).

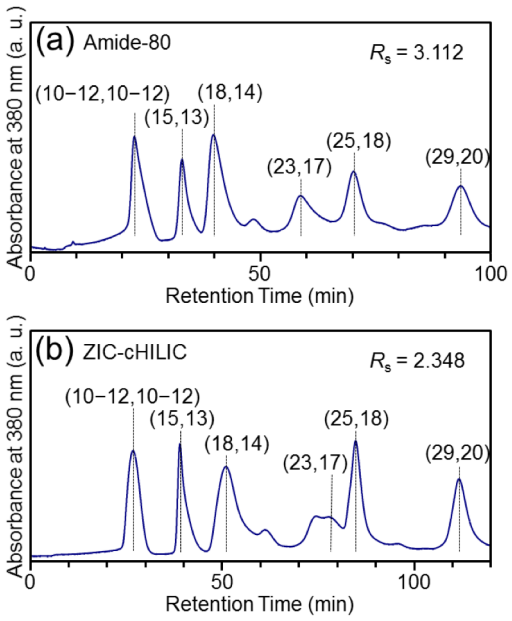

Figure S7. Dependence of the chromatograms of $Au_n(SG)_m$ clusters on the column. (a) Amide-80 and (b) ZIC-cHILIC columns. R_s indicates the resolution estimated using peaks of $Au_{10–12}(SG)_{10–12}$ and $Au_{15}(SG)_{13}$.[6] In the chromatogram, the peak position of each $Au_n(SG)_m$ cluster is described in the form of (n, m).

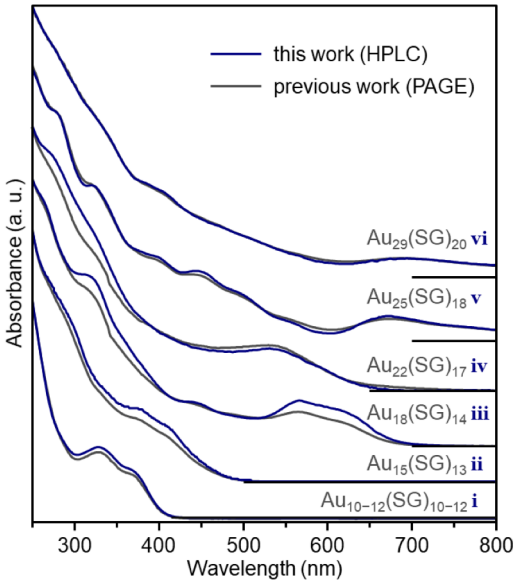

Figure S8. Comparison of optical absorption spectra of $Au_n(SG)_m$ clusters between (blue) **i**–**vi** in Figure 1 and (gray) the literature.[3] The chemical compositions reported in the literature[3] are shown in gray.

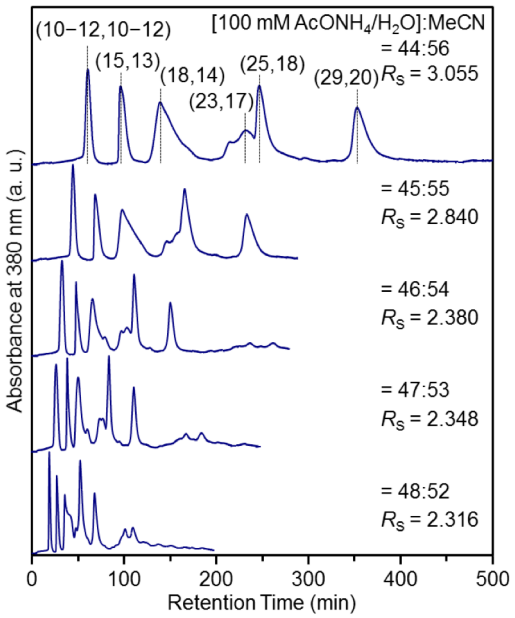

Figure S9. Dependence of the chromatograms of $Au_n(SG)_m$ clusters on the mobile phase in the experiments using a ZIC-cHILIC column. R_s indicates the resolution estimated using peaks of $Au_{10–12}(SG)_{10–12}$ and $Au_{15}(SG)_{13}$.[6] In the chromatogram, the peak position of each $Au_n(SG)_m$ cluster is described in the form of (n, m).

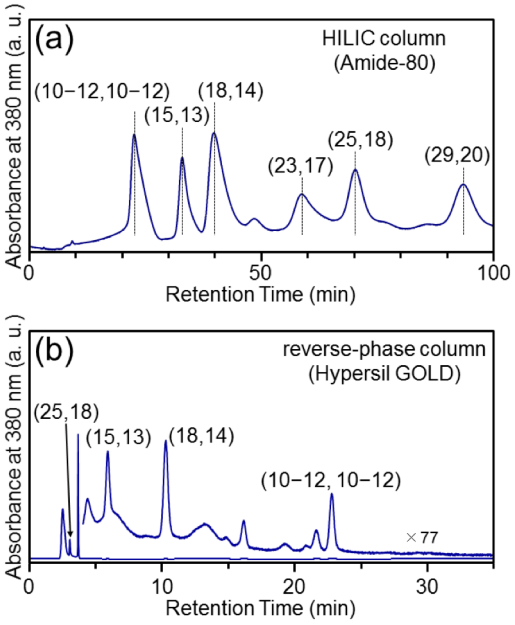

Figure S10. Comparison of the obtained chromatograms between (a) this work using the Amide-80 column and (b) previous work using a reverse-phase column (Hypersil GOLD) without an ion-pair reagent.[7] The chromatogram obtained using the Amide-80 column shows the opposite elution order to that obtained using the reverse-phase column, demonstrating that the $Au_n(SG)_m$ clusters were separated into each cluster type by the HILIC mode[2] in this study.

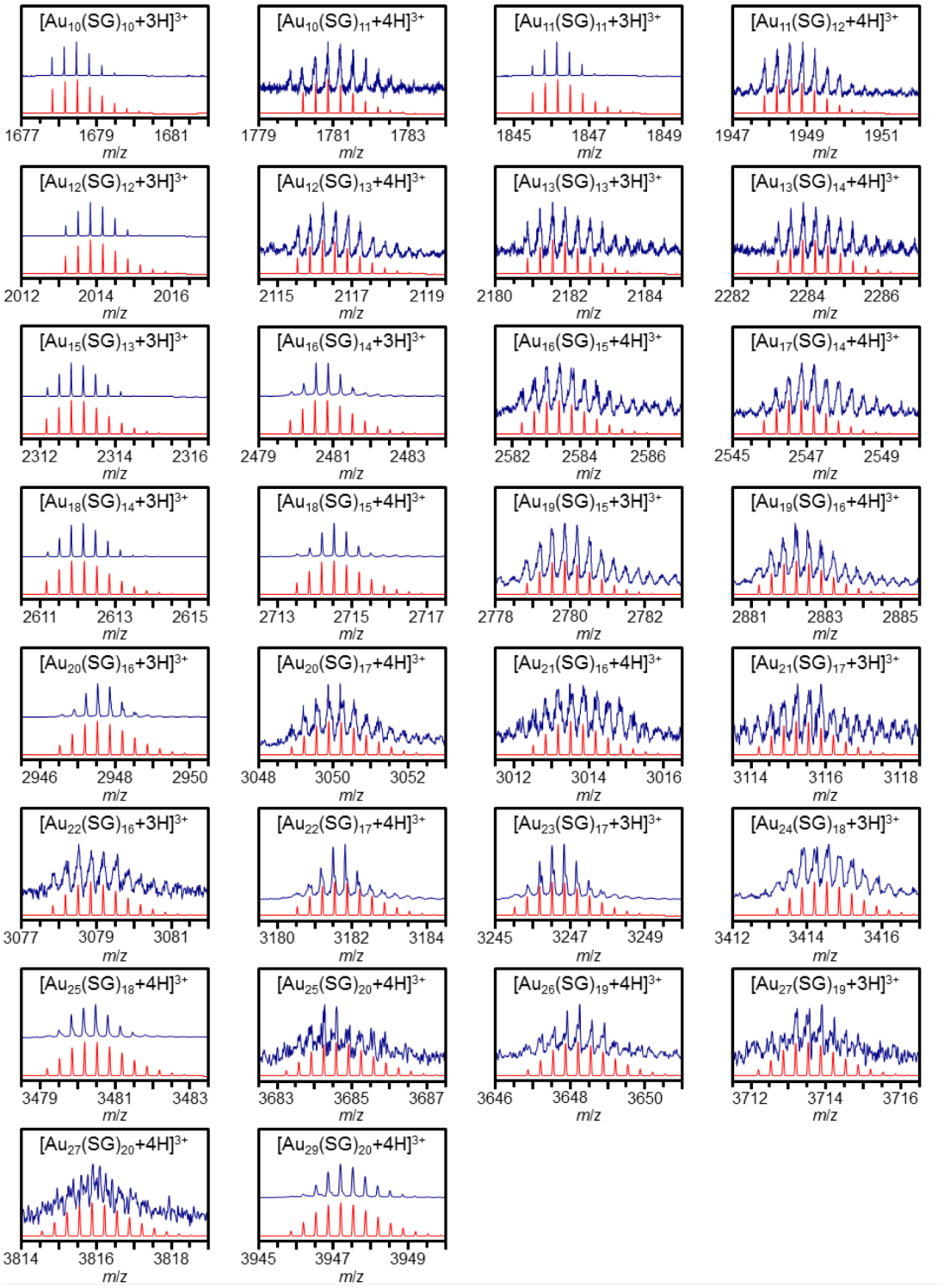

Figure S11. Enlarged positive-ion ESI mass spectra of $Au_n(SG)_m$ clusters (n = 10–29) used for Figure 4 (Table S1). Because both negative- and positive-ion ESI mass spectra showed the same chemical compositions for the same $Au_n(SG)_m$ clusters (Figure 1 and 2), the chemical compositions of $Au_n(SG)_m$ clusters used in Figure 4 were estimated using positive-ion ESI mass spectrometry as it has a high signal/noise ratio (Figure 2). In this experiment, the mobile phase was gradually changed using a linear gradient program from a mixture of 100-mM $AcONH_4$ aqueous solution and MeCN (50:50) to a mixture of 100-mM $AcONH_4$ aqueous solution and MeCN (84:16) with 380 min. This gradient elution was carried out to elute the larger $Au_n(SG)_m$ clusters within a narrow retention time and thereby increase the intensity of their ion peaks in the mass spectra.

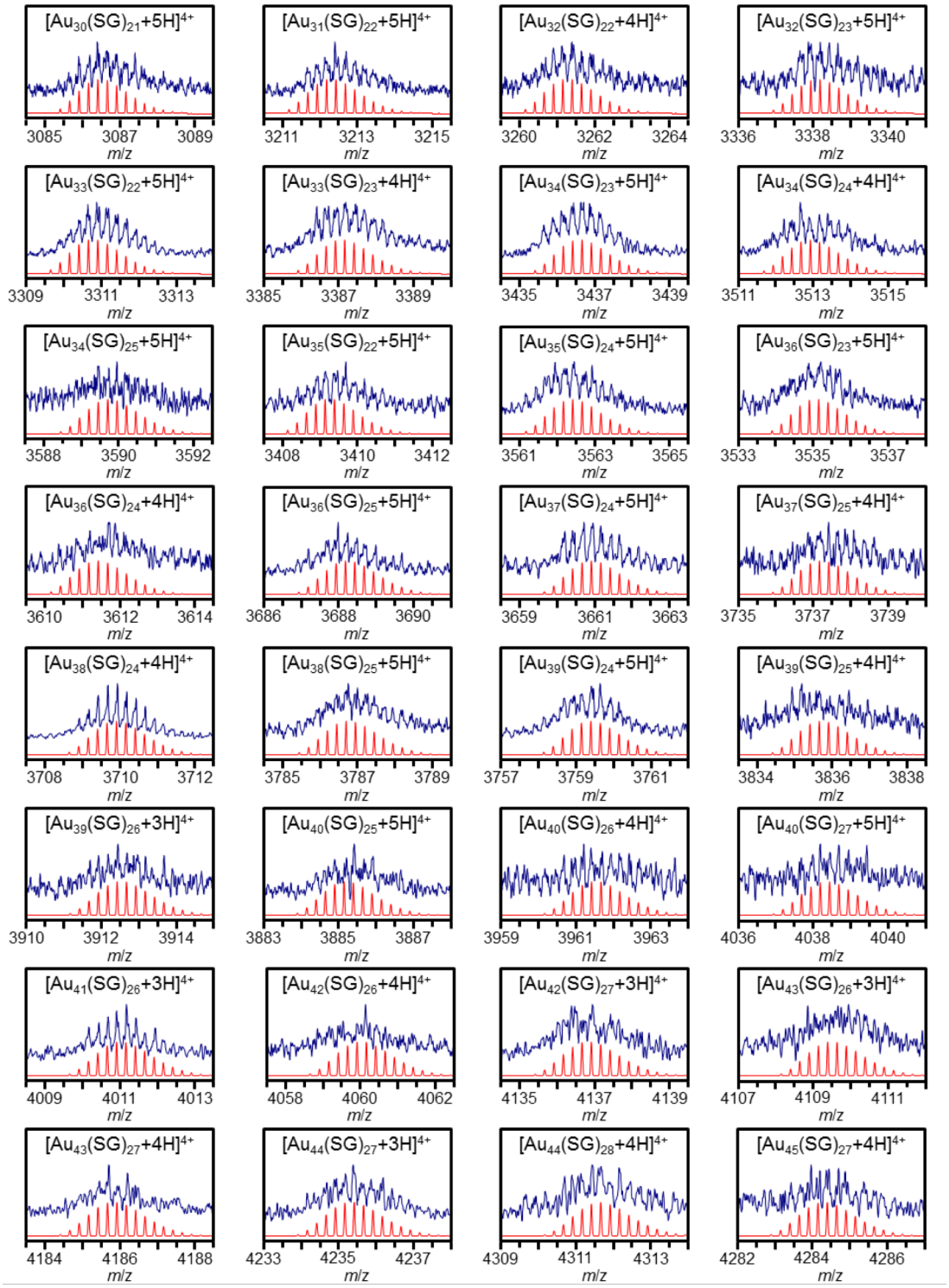

Figure S12. Enlarged positive-ion ESI mass spectra of $Au_n(SG)_m$ clusters (n = 30–45) used for Figure 4 (Table S1). Because both negative- and positive-ion ESI mass spectra showed the same chemical compositions for the same $Au_n(SG)_m$ clusters (Figure 1 and 2), the chemical compositions of $Au_n(SG)_m$ clusters used in Figure 4 were estimated using positive-ion ESI mass spectrometry as it has a high signal/noise ratio (Figure 2). In this experiment, the mobile phase was gradually changed using a linear gradient program from a mixture of 100-mM $AcONH_4$ aqueous solution and MeCN (50:50) to a mixture of 100-mM $AcONH_4$ aqueous solution and MeCN (84:16) with 380 min. This gradient elution was carried out to elute the larger $Au_n(SG)_m$ clusters within a narrow retention time and thereby increase the intensity of their ion peaks in the mass spectra. For the larger $Au_n(SG)_m$ clusters (n > 39), it was difficult to estimate the charge state without ambiguity (Table S1).

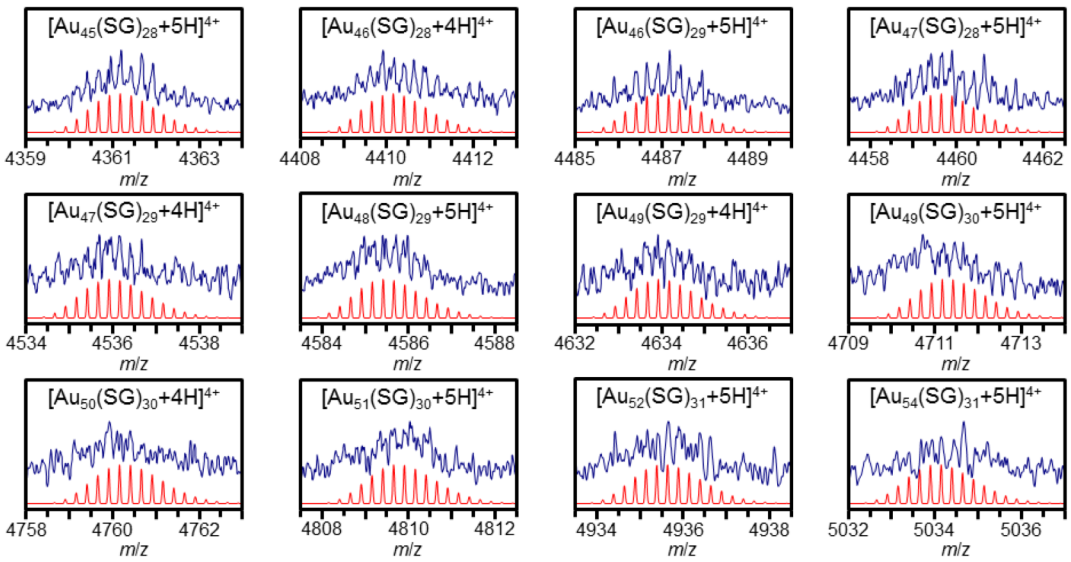

Figure S13. Enlarged positive-ion ESI mass spectra of $Au_n(SG)_m$ clusters (n = 45–54) used for Figure 4 (Table S1). Because both negative- and positive-ion ESI mass spectra showed the same chemical compositions for the same $Au_n(SG)_m$ clusters (Figure 1 and 2), the chemical compositions of $Au_n(SG)_m$ clusters used in Figure 4 were estimated using positive-ion ESI mass spectrometry as it has a high signal/noise ratio (Figure 2). To observe these clusters, the mobile phase was gradually replaced using a linear gradient program from a mixture of 100-mM $AcONH_4$ aqueous solution and MeCN (50:50) to a mixture of 100-mM $AcONH_4$ aqueous solution and MeCN (84:16) with 380 min. This gradient elution was carried out to elute the larger $Au_n(SG)_m$ clusters within a narrow retention time and thereby increase the intensity of their ion peaks in the mass spectra. For these larger $Au_n(SG)_m$ clusters, it was difficult to estimate the charge state without ambiguity (Table S1).

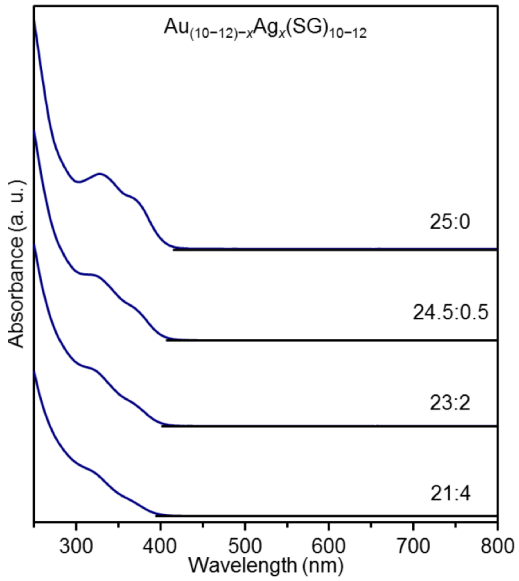

Figure S14. Optical absorption spectra observed using a PDA for $Au_{(10-12)-x}Ag_x(SG)_{10-12}$ clusters prepared with metal ion ratios of $[HAuCl_4]$:$[AgNO_3]$ of 25:0, 24.5:0.5, 23:2, and 21:4.

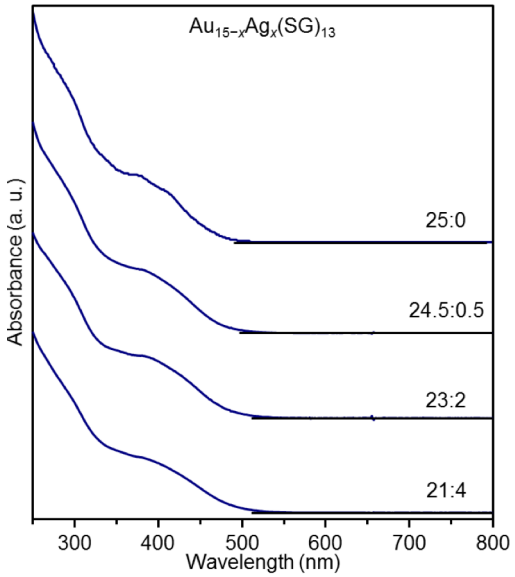

Figure S15. Optical absorption spectra observed using a PDA for $Au_{15-x}Ag_x(SG)_{13}$ clusters prepared with metal ion ratios of $[HAuCl_4]$:$[AgNO_3]$ of 25:0, 24.5:0.5, 23:2, and 21:4.

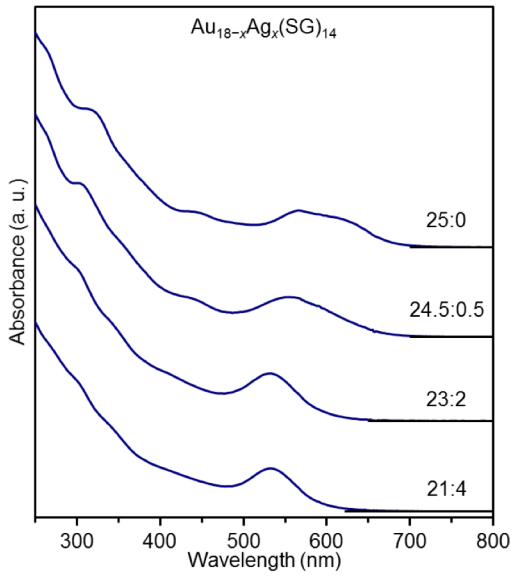

Figure S16. Optical absorption spectra observed using a PDA for $Au_{18-x}Ag_x(SG)_{14}$ clusters prepared with metal ion ratios of $[HAuCl_4]$:$[AgNO_3]$ of 25:0, 24.5:0.5, 23:2, and 21:4. The observed structural change depending on the ion ratios is consistent with that reported by Xie and co-workers.[8]

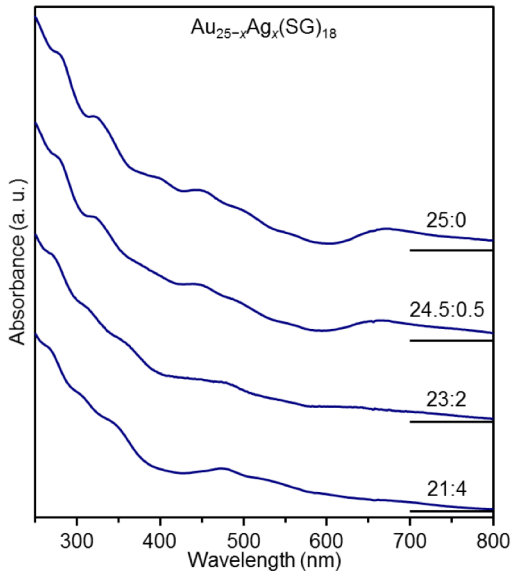

Figure S17. Optical absorption spectra observed using a PDA for $Au_{25-x}Ag_x(SG)_{18}$ clusters prepared with metal ion ratios of $[HAuCl_4]$:$[AgNO_3]$ of 25:0, 24.5:0.5, 23:2, and 21:4. The observed structural change depending on the ion ratio is consistent with that reported by Xie and co-workers for $Au_{25-x}Ag_x(SR)_{18}$ (R = 6-mercaptohexanoic acid, etc.).[9]

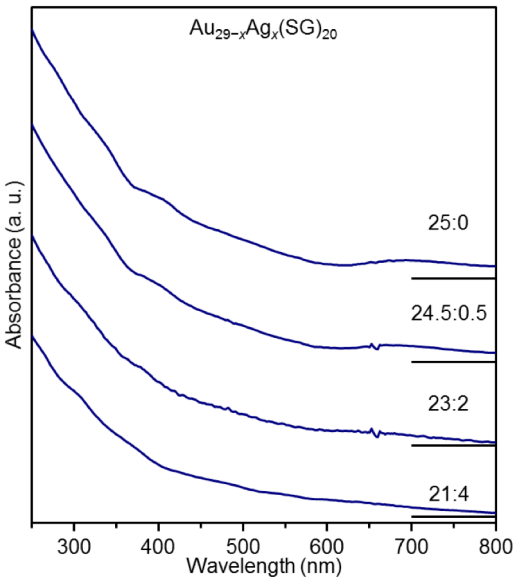

Figure S18. Optical absorption spectra observed using a PDA for $Au_{29-x}Ag_x(SG)_{20}$ clusters prepared with metal ion ratios of $[HAuCl_4]$:$[AgNO_3]$ of 25:0, 24.5:0.5, 23:2, and 21:4.

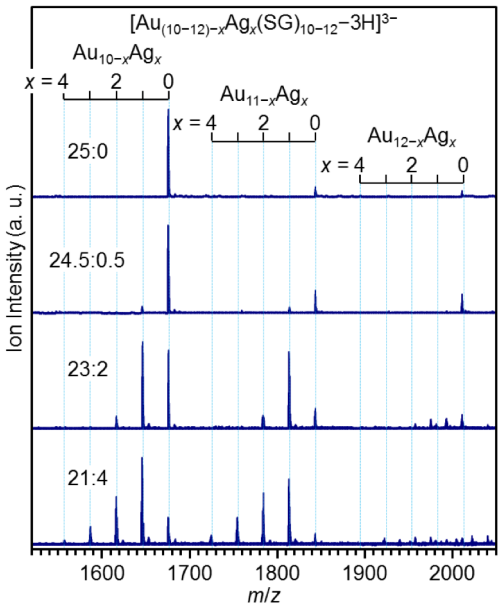

Figure S19. Assignments of negative-ion ESI mass spectra of $[Au_{(10–12)–x}Ag_x(SG)_{10–12}–3H]^{3–}$.

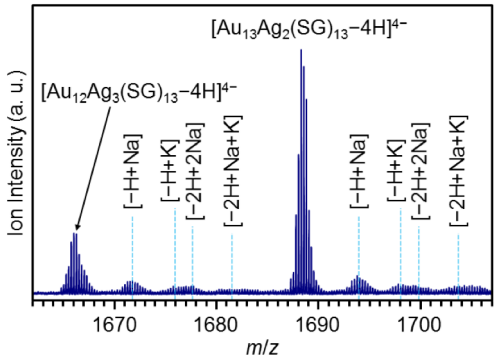

Figure S20. Assignments of negative-ion ESI mass spectrum of $[Au_{15–x}Ag_x(SG)_{13}–4H]^{4–}$ ($x = 2, 3$) prepared with a metal ion ratio of $[HAuCl_4]$:$[AgNO_3]$ of 23:2.

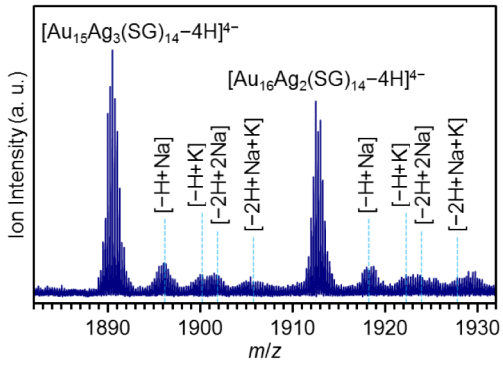

Figure S21. Assignments of negative-ion ESI mass spectrum of $[Au_{18–x}Ag_x(SG)_{14}–4H]^{4–}$ ($x = 2, 3$) prepared with a metal ion ratio of $[HAuCl_4]$:$[AgNO_3]$ of 23:2.

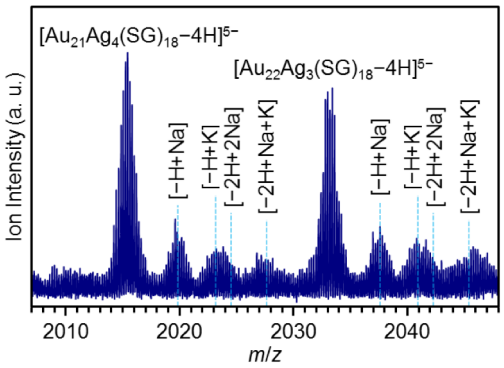

Figure S22. Assignments of negative-ion ESI mass spectrum of $[Au_{25-x}Ag_x(SG)_{18}-4H]^{5-}$ ($x = 3, 4$) prepared with a metal ion ratio of $[HAuCl_4]$:$[AgNO_3]$ of 23:2.

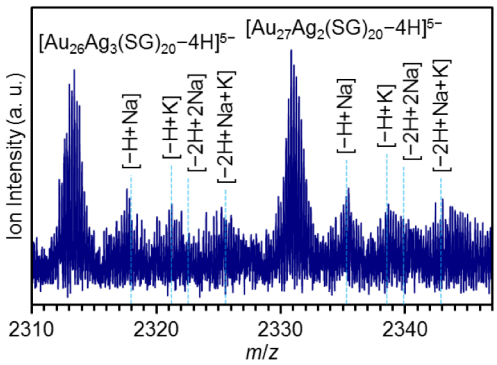

Figure S23. Assignments of negative-ion ESI mass spectrum of $[Au_{29-x}Ag_x(SG)_{20}-4H]^{5-}$ ($x = 2, 3$) prepared with a metal ion ratio of $[HAuCl_4]$:$[AgNO_3]$ of 23:2.

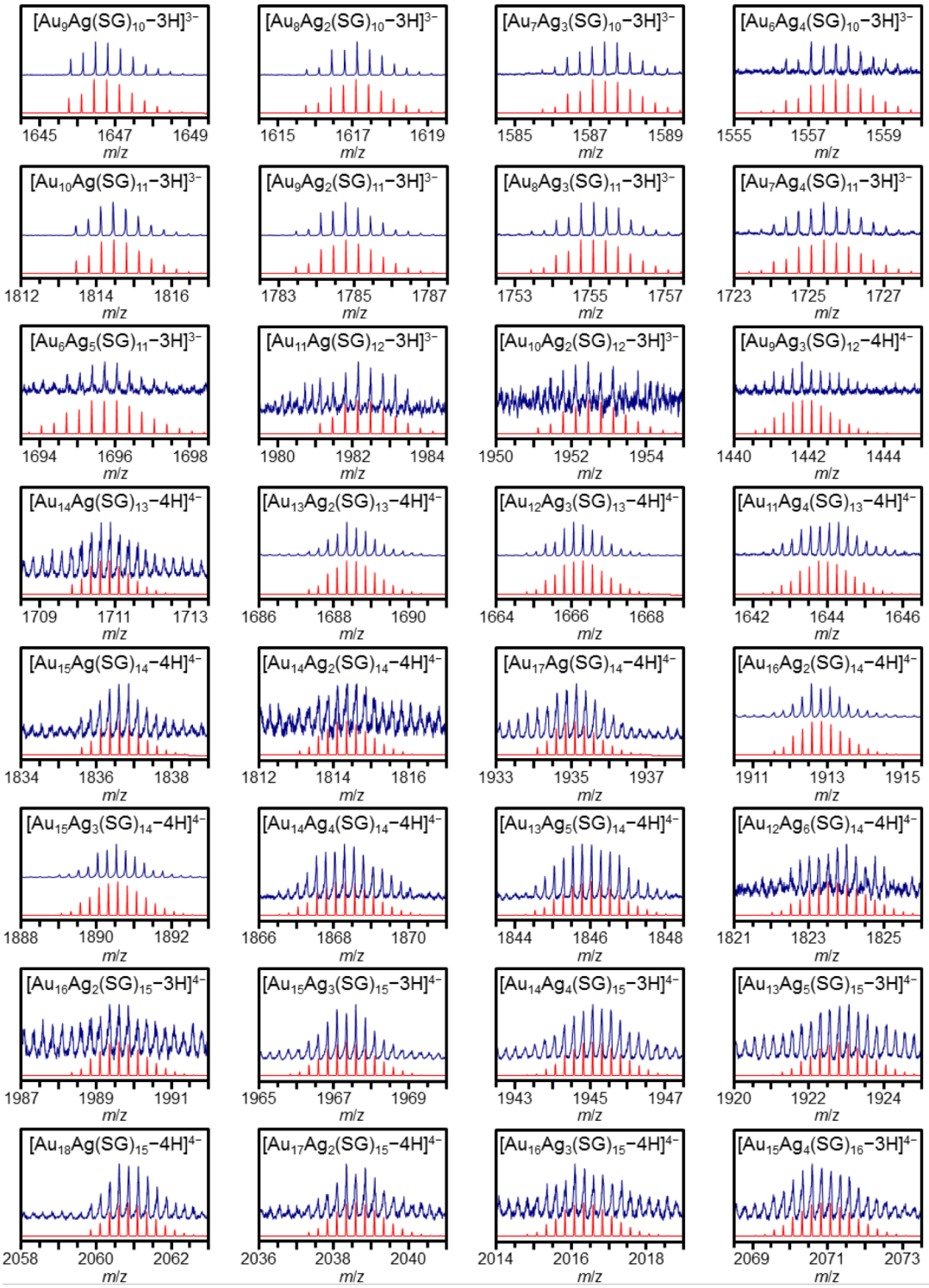

Figure S24. Enlarged negative-ion ESI mass spectra of $Au_{n-x}Ag_x(SG)_m$ clusters (n = 10–19; Table S2). In this experiment, the mobile phase was flowed with a constant mixing ratio (isocratic mode).

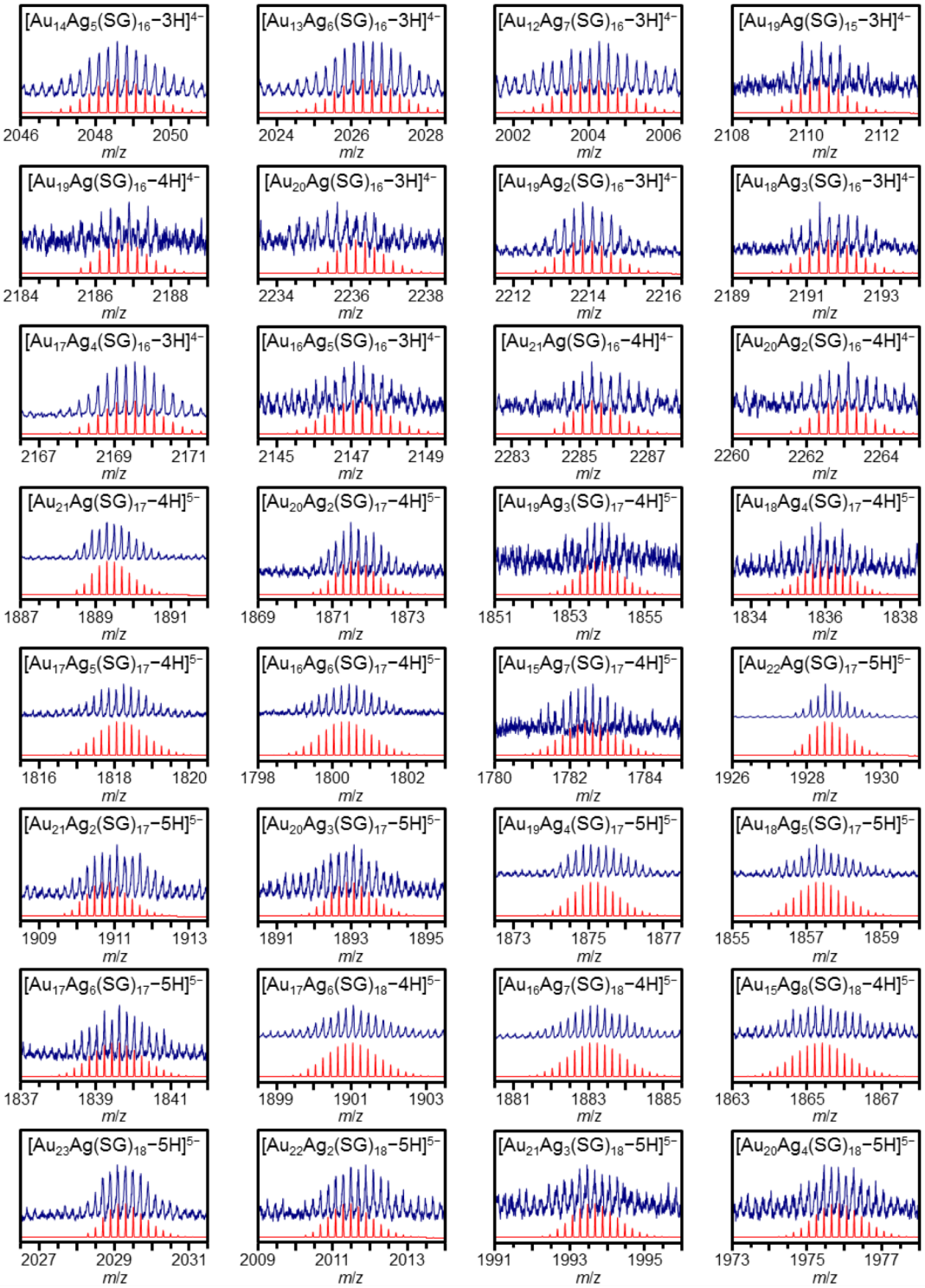

Figure S25. Enlarged negative-ion ESI mass spectra of $Au_{n-x}Ag_x(SG)_m$ clusters (n = 19–24; Table S2). In this experiment, the mobile phase was flowed with a constant mixing ratio (isocratic mode).

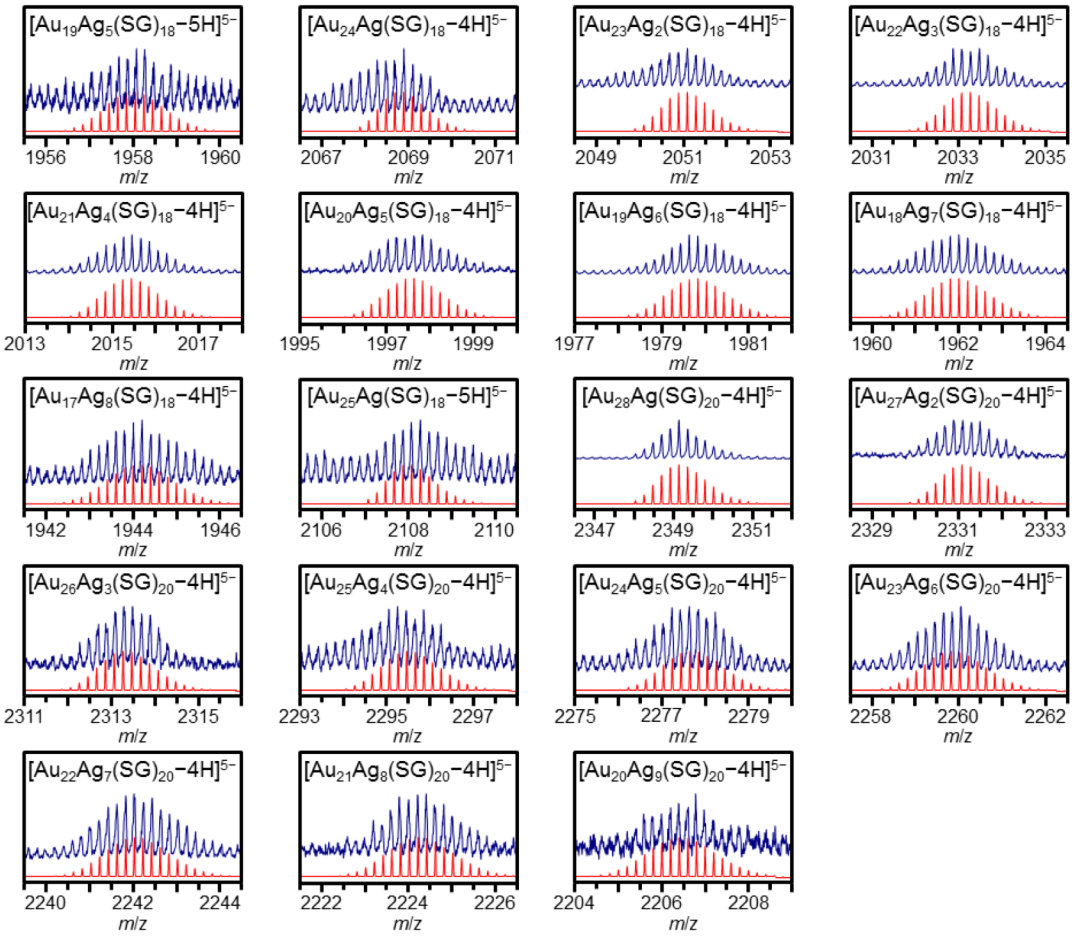

Figure S26. Enlarged negative-ion ESI mass spectra of $Au_{n-x}Ag_x(SG)_m$ clusters (n = 24–29; Table S2). In this experiment, the mobile phase was flowed with a constant mixing ratio (isocratic mode).

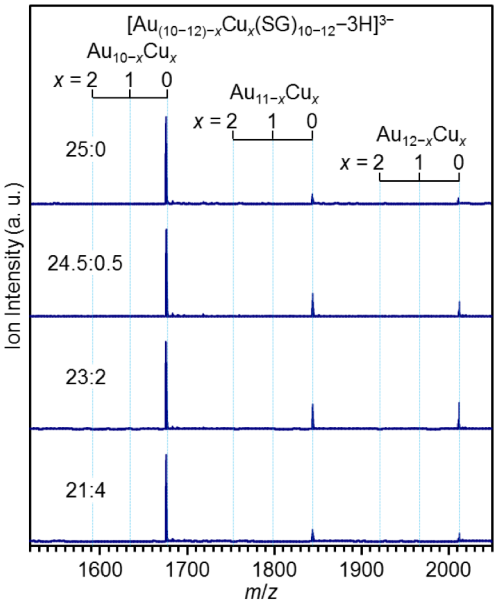

Figure S27. Assignments of negative-ion ESI mass spectra of $[Au_{(10–12)–x}Cu_x(SG)_{10–12}–3H]^{3–}$.

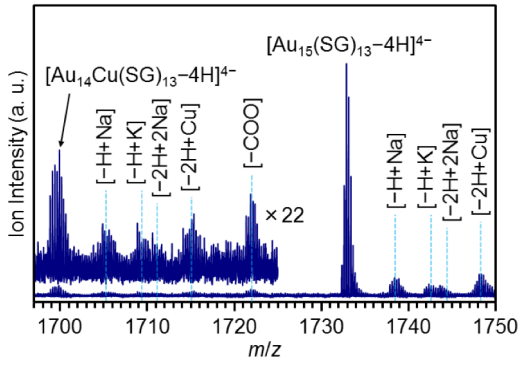

Figure S28. Assignments of negative-ion ESI mass spectrum of $[Au_{15–x}Cu_x(SG)_{13}–4H]^{4–}$ ($x = 0, 1$) prepared with a metal ion ratio of $[HAuCl_4]$:$[CuCl_2]$ of 21:4.

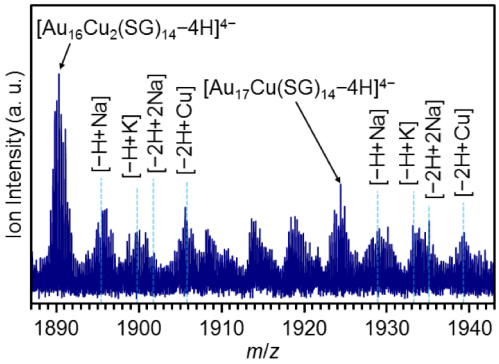

Figure S29. Assignments of negative-ion ESI mass spectrum of $[Au_{18–x}Cu_x(SG)_{14}–4H]^{4–}$ ($x = 1, 2$) prepared with a metal ion ratio of $[HAuCl_4]$:$[CuCl_2]$ of 21:4.

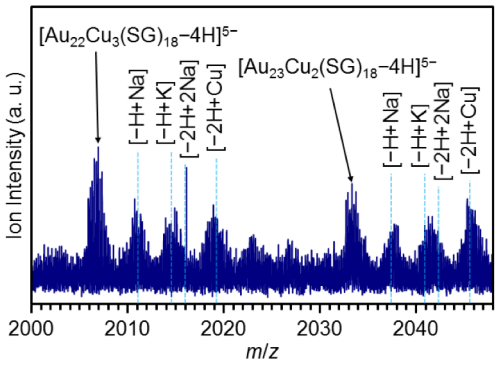

Figure 30. Assignments of negative-ion ESI mass spectrum of $[Au_{25-x}Cu_x(SG)_{18}-4H]^{5-}$ (x = 2, 3) prepared with a metal ion ratio of $[HAuCl_4]$:$[CuCl_2]$ of 21:4.

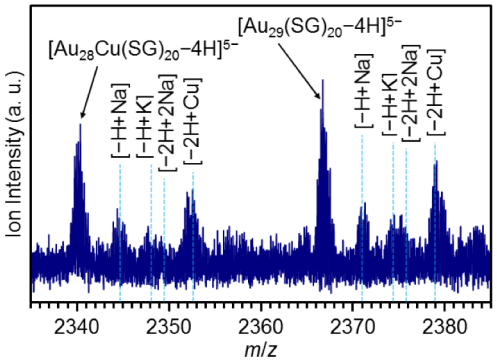

Figure S31. Assignments of negative-ion ESI mass spectrum of $[Au_{29-x}Cu_x(SG)_{20}-4H]^{5-}$ (x = 0, 1) prepared with a metal ion ratio of $[HAuCl_4]$:$[CuCl_2]$ of 21:4.

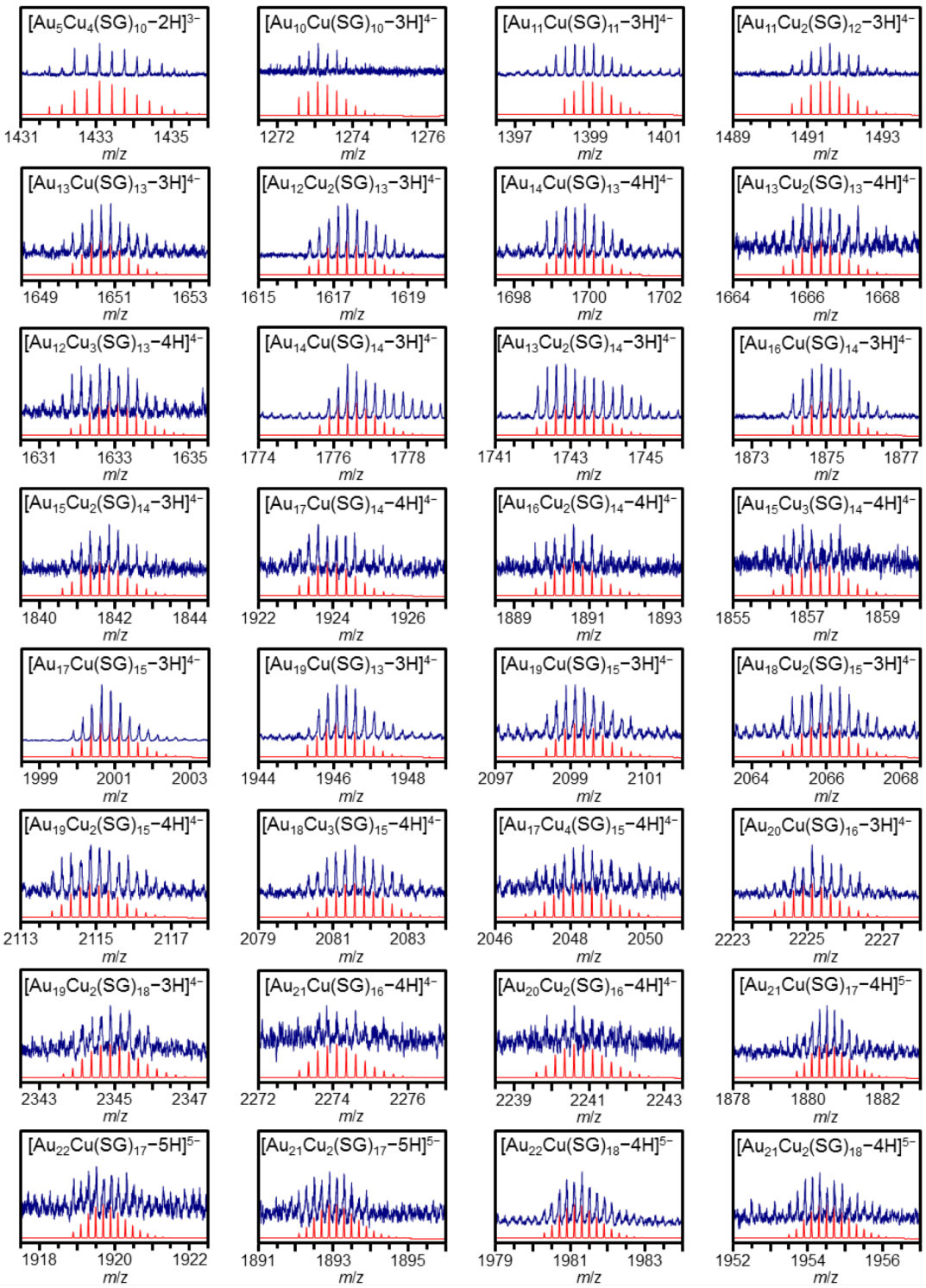

Figure S32. Enlarged negative-ion ESI mass spectra of $Au_{n-x}Cu_x(SG)_m$ clusters (n = 9–23; Table S3). In this experiment, the mobile phase was flowed with a constant mixing ratio (isocratic mode).

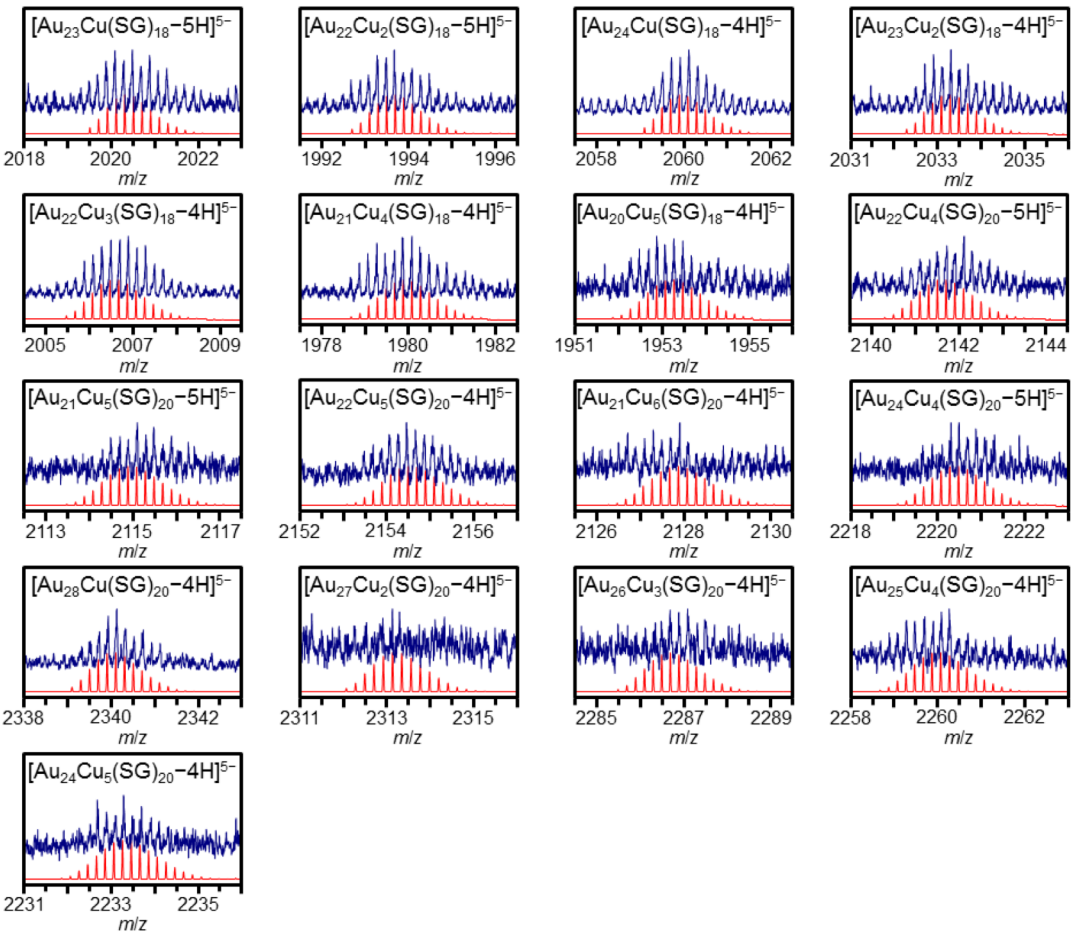

Figure S33. Enlarged negative-ion ESI mass spectra of $Au_{n-x}Cu_x(SG)_m$ clusters (n = 23–29; Table S3). In this experiment, the mobile phase was flowed with a constant mixing ratio (isocratic mode).

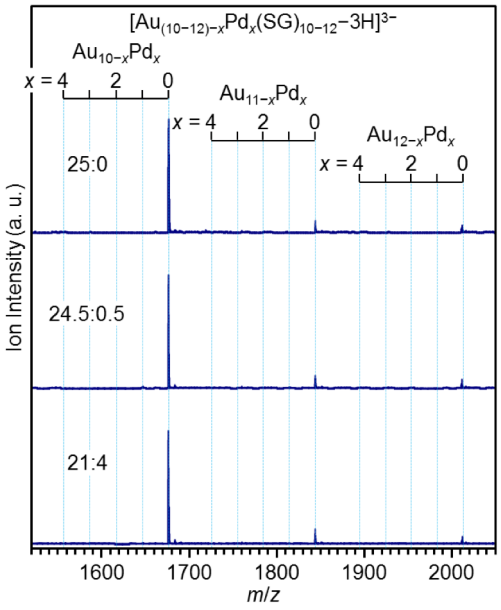

Figure S34. Assignments of negative-ion ESI mass spectra of $[Au_{(10–12)–x}Pd_x(SG)_{10–12}–3H]^{3–}$.

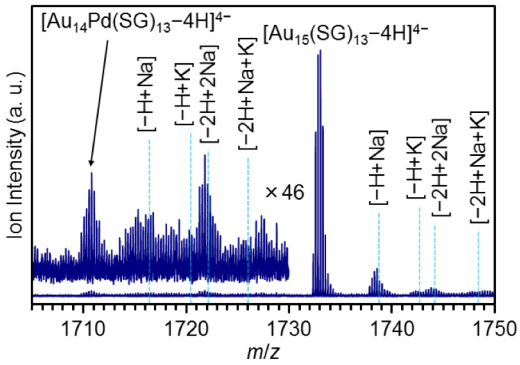

Figure S35. Assignments of negative-ion ESI mass spectrum of $[Au_{15–x}Pd_x(SG)_{13}–4H]^{4–}$ (x = 0, 1) prepared with a metal ion ratio of $[HAuCl_4]$:$[PdCl_2·2NaCl]$ of 21:4.

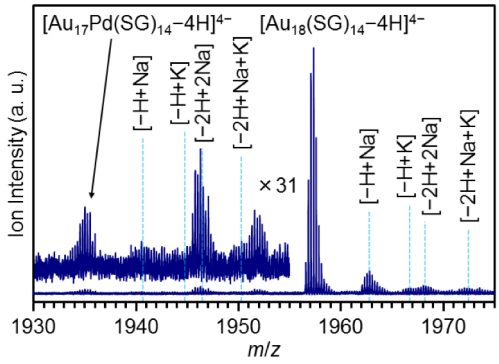

Figure S36. Assignments of negative-ion ESI mass spectrum of $[Au_{18-x}Pd_x(SG)_{14}-4H]^{4-}$ (x = 0, 1) prepared with a metal ion ratio of $[HAuCl_4]$:$[PdCl_2 \cdot 2NaCl]$ of 21:4.

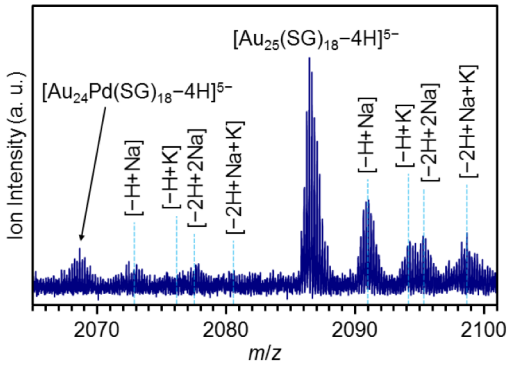

Figure S37. Assignments of negative-ion ESI mass spectrum of $[Au_{25-x}Pd_x(SG)_{18}-4H]^{5-}$ (x = 0, 1) prepared with a metal ion ratio of $[HAuCl_4]$:$[PdCl_2 \cdot 2NaCl]$ of 21:4.

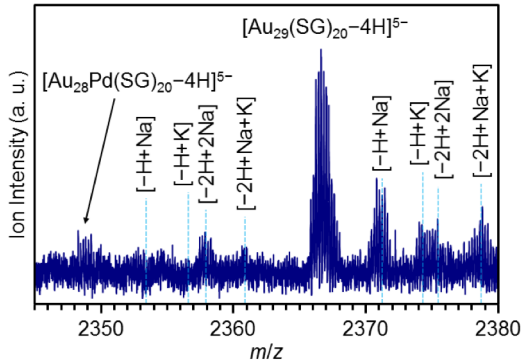

Figure S38. Assignments of negative-ion ESI mass spectrum of $[Au_{29-x}Pd_x(SG)_{20}-4H]^{5-}$ (x = 0, 1) prepared with a metal ion ratio of $[HAuCl_4]$:$[PdCl_2 \cdot 2NaCl]$ of 21:4.

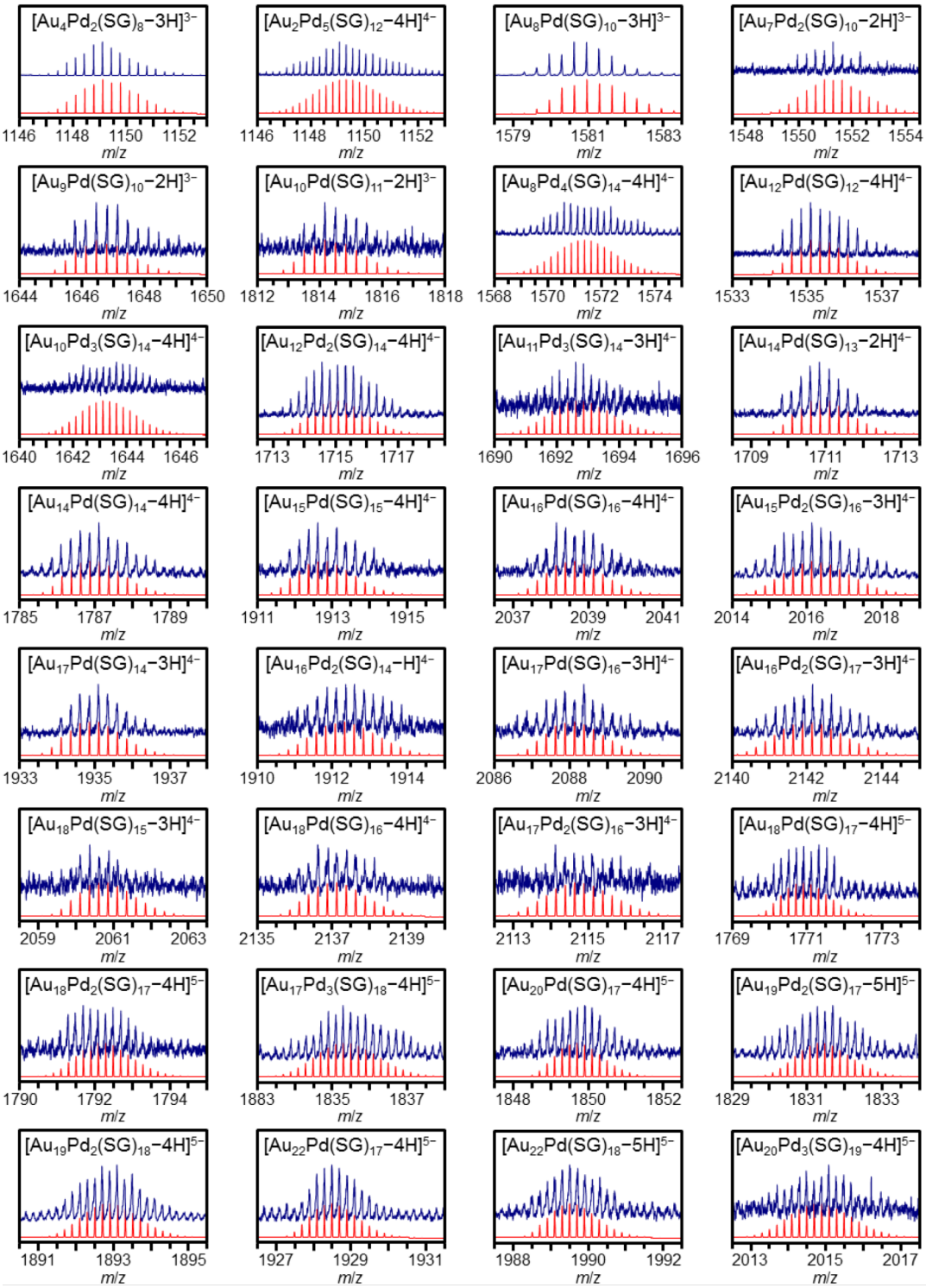

Figure S39. Enlarged negative-ion ESI mass spectra of $Au_{n-x}Pd_x(SG)_m$ clusters (n = 6–23; Table S4). In this experiment, the mobile phase was flowed with a constant mixing ratio (isocratic mode).

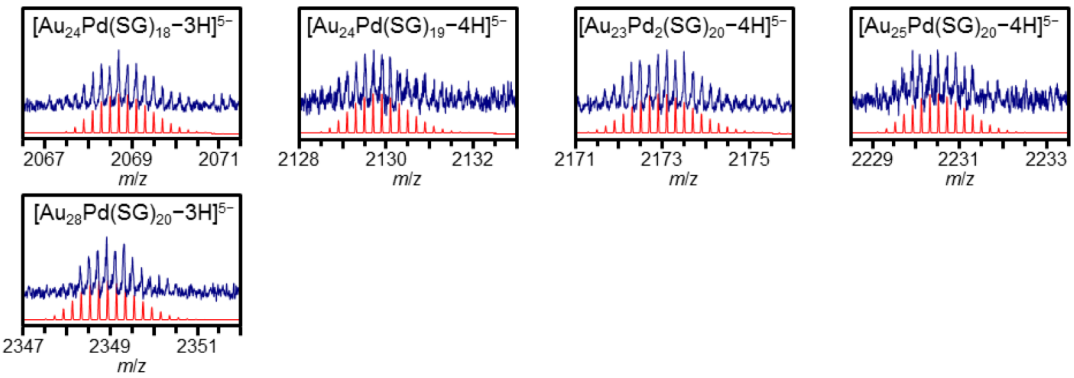

Figure S40. Enlarged negative-ion ESI mass spectra of $Au_{n-x}Pd_x(SG)_m$ clusters (n = 25–29; Table S4). In this experiment, the mobile phase was flowed with a constant mixing ratio (isocratic mode).

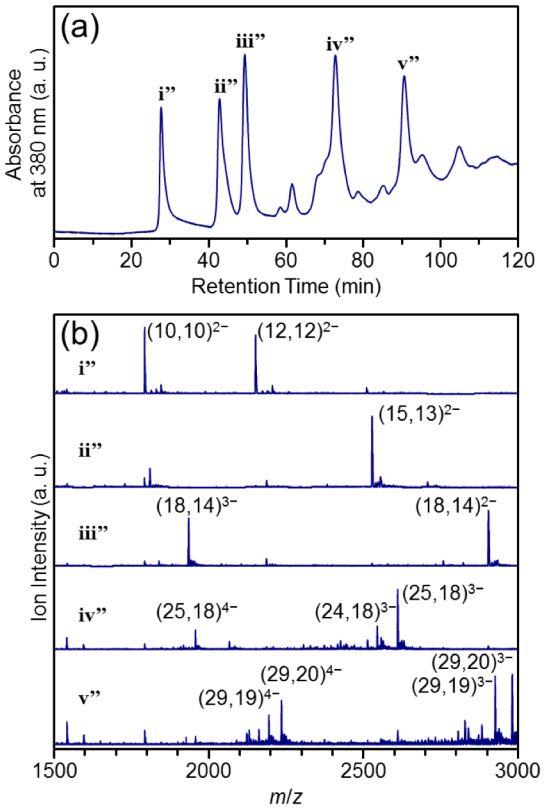

Figure S41. (a) UV chromatogram obtained for $Au_n(NALC)_m$ clusters using LC/MS with an Amide-80 column and (b) negative-ion ESI mass spectra of fractions **i"**–**v"** in the UV chromatogram in (a). In this study, the mobile phase was gradually replaced using a linear gradient program from a mixture of 100-mM $AcONH_4$ aqueous solution and MeCN (43:57) to a mixture of 100-mM $AcONH_4$ aqueous solution and MeCN (73:27) with 600 min. This gradient elution was carried out to elute the larger $Au_n(NALC)_m$ clusters within a narrow retention time and thereby increase the intensity of their ion peaks in the mass spectra. In (b), only the main peaks are assigned. The notation $(n, m)^{z-}$ indicates $[Au_n(NALC)_m]^{z-}$. For these clusters, the charge states of the metal core could not be determined because of the limited resolution of the quadrupole mass spectrometer (Waters, SQD2) used in this work.

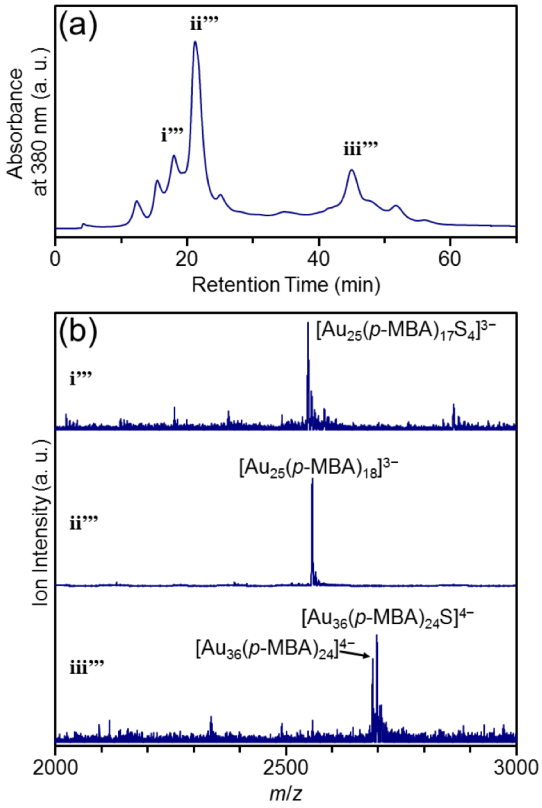

Figure S42. (a) UV chromatogram obtained for $Au_n(p\text{-MBA})_m$ clusters using LC/MS with an Amide-80 column and (b) negative-ion ESI mass spectra of peaks **i'''**–**iii'''** in the UV chromatogram in (a). In this study, the mobile phase was gradually replaced using a linear gradient program from a mixture of 100-mM $AcONH_4$ aqueous solution and MeCN (45:55) to a mixture of 100-mM $AcONH_4$ aqueous solution and MeCN (75:25) with 300 min. This gradient elution was carried out to elute the larger $Au_n(p\text{-MBA})_m$ clusters within a narrow retention time and thereby increase the intensity of their ion peaks in the mass spectra. In (b), only the main peaks are assigned. For these clusters, the charge states of the metal core could not be determined because of the limited resolution of the quadrupole mass spectrometer (Waters, SQD2) used in this work.

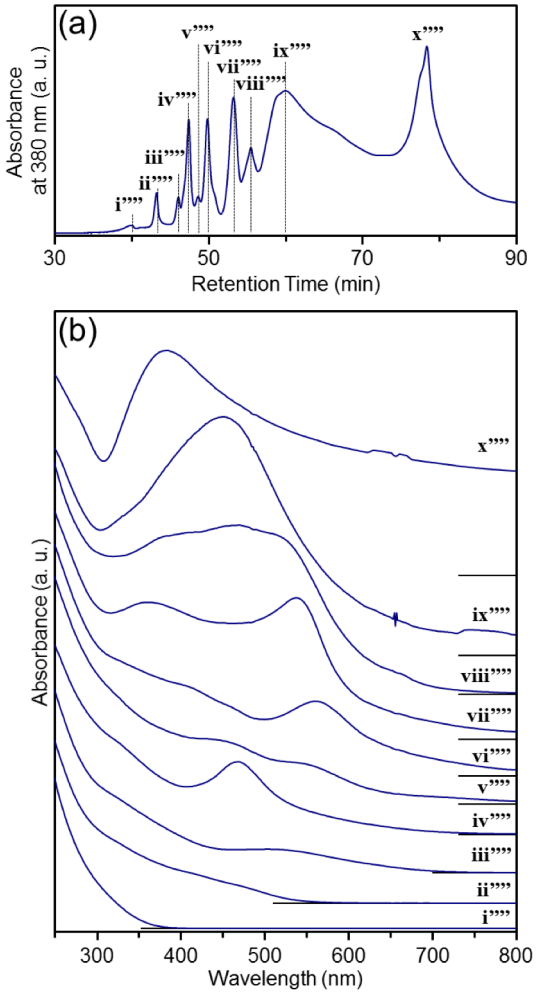

Figure S43. (a) UV chromatogram obtained for $Ag_n(SG)_m$ clusters using LC with an Amide-80 column and (b) optical absorption spectrum of each peak (**i''''**–**x''''**). In this study, the mobile phase was gradually replaced using a linear gradient program from a mixture of 100-mM $AcONH_4$ aqueous solution and MeCN (40:60) to a pure 100-mM $AcONH_4$ aqueous solution with 120 min.

4. References

(1) M. Walter, J. Akola, O. Lopez-Acevedo, P. D. Jadzinsky, G. Calero, C. J. Ackerson, R. L. Whetten, H. Grönbeck and H. Häkkinen, *Proc. Natl. Acad. Sci. U. S. A.*, 2008, **105**, 9157−9162.

(2) B. Buszewski and S. Noga, *Anal. Bioanal. Chem.*, 2012, **402**, 231−247.

(3) Y. Negishi, K. Nobusada and T. Tsukuda, *J. Am. Chem. Soc.*, 2005, **127**, 5261−5270.

(4) M. M. F. Choi, A. D. Douglas and R. W. Murray, *Anal. Chem.*, 2006, **78**, 2779–2785.

(5) D. M. Black, M. M. Alvarez, F. Yan, W. P. Griffith, G. Plascencia-Villa, S. B. H. Bach and R. L. Whetten, *J. Phys. Chem. C*, 2017, **121**, 10851−10857.

(6) Y. Niihori, M. Matsuzaki, C. Uchida and Y. Negishi, *Nanoscale*, 2014, **6**, 7889–7896.

(7) Y. Niihori, Y. Kikuchi, D. Shima, C. Uchida, S. Sharma, S. Hossain, W. Kurashige and Y. Negishi, *Ind. Eng. Chem. Res.*, 2017, **56**, 1029−1035.

(8) Y. Yu, Q. Yao, T. Chen, G. X. Lim and J. Xie, *J. Phys. Chem. C*, 2016, **120**, 22096−22102.

(9) X. Dou, X. Yuan, Q. Yao, Z. Luo, K. Zheng and J. Xie, *Chem. Commun.*, 2014, **50**, 7459−7462.